EXPERIMENTAL AND NUMERICAL INVESTIGATION OF THERMAL FIELD FOR A MOTOR AND RELATED FACTORS SENSITIVITIES USING COMBINED CFD-TAGUCHI METHOD

by

Xueqi LIANG[a], Huiqiang LUO[b], Min ZENG[a], Yining WU[a,*], and Qiuwang WANG[a]

[a]Key Laboratory of Thermo-Fluid Science and Engineering, MOE, Xi'an Jiaotong University, Shaanxi, China
[b]CRRC Yongji Electric Co., Ltd., Shanxi, China

Original scientific paper
https://doi.org/10.2298/TSCI19S4065L

Over-temperature is a fatal problem when a motor is running. In this work, the temperature and temperature rise of the motor are investigated experimentally and numerically. The experiment is conducted by means of both voltmeter-ammeter method and embedding thermal resistors, to obtain the mean temperature and the local temperature of the stator coils, respectively. The numerical calculation is carried out to study the temperature field of the stator and the rotor, which agrees well with the experimental result. What's more, the sensitivity analysis of eighteen factors to the temperature is investigated using combined CFD-Taguchi method. The main conclusions are drawn. Firstly, according to the numerical results, the maximal temperature and the maximal temperature rise at rated speed are 143 ℃ and 99 K, respectively. The values are 145.8 ℃ and 90 K, according to the experimental results, which are lower than the temperature allowed, 180 ℃ and temperature rise allowed, 125 K. Secondly, the sensitivity analysis results suggest that the key factors influencing the temperature are in sequence the ambient temperature, the copper loss, the thickness of the layers, the outside convection heat transfer coefficient of crate, the iron loss at the tooth and thermal conductivity of the insulation. The contact thermal resistance and the thermal conductivity of the core in axial direction have little influence on the temperature. The rank to the temperature rise is similar except the ambient temperature, which has little effect on the temperature rise.

Key words*: temperature rise, motor, Taguchi method, sensitivity analysis, multiple moving reference frames, embedding thermal resistors*

Introduction

The motor used widely in household electrical appliances, industrial production, space power equipment and so on tends to be more compact and rotate faster, with the progress of science and technology. Then, the temperature of the motor goes up and the heat release becomes harder, which may cause that the temperature of stator windings exceed the limit allowed. Then the motor burns out [1] and the product breaks out. So there is a big ne-

* Corresponding author, email: ynwu@mail.xjtu.edu.cn

cessity to do the thermal analysis of the motor, which are investigated mainly by the means of experiment, thermal network, and numerical simulation.

Živan *et al*. [2] studied the mean temperature of the stator wingdings, temperature of the rotor windings, and temperature of the motor housing by measuring electric parameters in experiment and calculating the resistance. The mean temperature could be derived. But the local temperature, especially the maximal temperature, and the location of peak temperature are difficult be to known by the voltmeter-ammeter method in experiment.

Meng *et al.* [3] and Wen *et al*. [4] Claudio *et al.* [5], Zhang *et al.* [6, 7], Bogumi *et al.*[8], Yabiku *et al.*[9], and Hirano *et al.* [10] investigated the temperature rise of the motor by establishing the thermal network. Meng *et al.* [3] and Wen *et al*. [4] got the flow rate by building the wind network first. Then he derived the change of the mean temperature of stator and rotor by calculating the thermal network coupled with the flow obtained in the wind network when the motor being launched. However, the accurate temperature field could not be depicted by equivalent heat circuit model.

Numerical simulation was also adopted to study the thermal characteristics of the motor. Thermal analysis of local parts of motor, such as the teeth, magnet, isolating, rotor, stator yoke was investigated by Mohamed *et al.* [11]. The influences of other parts have been neglected. Zhu *et al.* [12] investigated the temperature field of the stator and rotor by building a coupled field-circuit thermal model. Only one tooth of the motor was studied simplifying the motor to a symmetrical model. So the asymmetry of stator windings, fan, dust filter and so on could not be taken into account.

Kim *et al.* [13] and Wang *et al.* [14] did optimization using Taguchi method to obtain more average operational torque (AOT) and reduce torque ripple than the prototype based on the finite element method (FEM). The sensitivity analysis about temperature was barely investigated.

This work investigates experimentally the temperature field of a metro motor by the method of voltmeter-ammeter method and embedding thermal resistors, to get the mean temperature rise and the local temperature of the stator wingdings. Then, the numerical simulation is carried out to study the temperature field of both the stator and the rotor. So, the maximal temperature of the motor and where it located can be known, which is highly concerned during the operation. Furthermore, the sensitivity analysis of the main factors affecting the temperature and the temperature rise by Taguchi method is conducted to rank the contribution ratio. The results of the sensitivity analysis figure the significant factors, whose accuracy can be improved further to get preciser temperature field of motor.

Experimental investigation

Experimental system and test section

The experimental system for investigating the temperature rise of the motor is shown in fig. 1. The power supply system, the load system, the motor to research, the measuring system and the gear box consist of the experimental system. The power system contains a step-down transformer, a frequency converter, a sine wave filter and a boosting transformer. The step-down transformer changes the voltage from 10000 V into 690 V. Then the frequency converter changes the frequency from 50 Hz into other frequency to change the speed of the motor. The filter moves out the harmonic wave and the transformer raises the voltage. Then the power is supplied to the motor to be researched, which the load system is connected with through the gear box. The load system consists of two electric generators, a DC inverter and a

boosting transformer. The DC inverter changes the alternating current into direct current and the transformer raises the voltage to 10000 V. The temperature inspection instrument shows the temperature of the embedded thermal resistors. The torque and speed sensor are connected to the motor with a coupling, to measure the speed and torque of the motor.

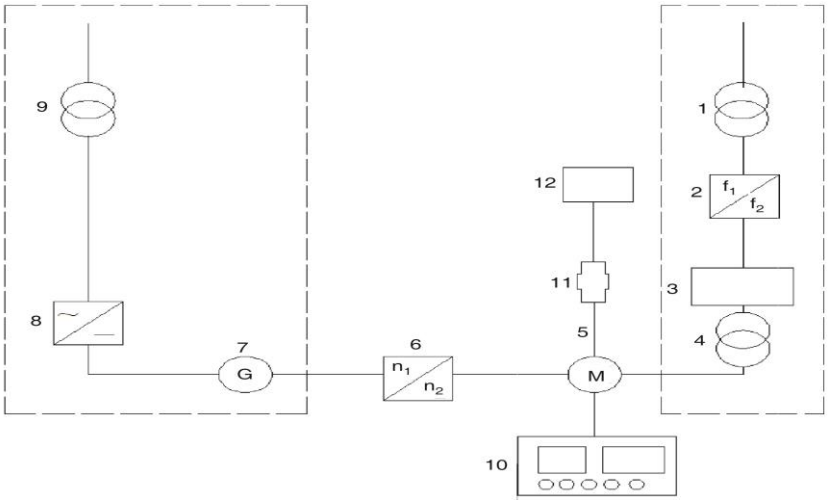

Figure. 1 Schematic of experiment set-up; *1, 4, 9 – transformer, 2 – frequency converter, 3 – sine wave filter, 5 – motor to research, 6 – gear box, 7 – electric generator, 8 – DC inverter, 10 – temperature inspection instrument, 11 – coupling, 12 – torque and speed sensor*

There are two methods adopted to study the temperature rise of the motor. The mean temperature rise is obtained by the way of voltammetry while the local temperature rises by the means of embedding thermal resistors.

The experimental procedures of the voltammetry and embedding thermal resistors are as follows.

- the direct resistance at cold state is measured firstly,
- the support bench is set up to support the motor and make sure the motor and the electric generator are at the same height,
- the measuring system is set-up, containing the coupling, the speed and torque sensor and so on,
- when the temperature shown on the temperature inspection instrument varies less than 2 ºC in 1 hour, it is conceived that the motor is at the thermal steady-state,
- the power is cut off and the motor brakes under the load,
- the indexing table is calibrated and the direct resistance at hot state is measured, and the temperature measured by embedding thermal resistors is shown on the temperature inspection instrument.

Data processing

Voltmeter-ammeter method, embedding thermal resistors

The line resistance at cold state between two phases derived from the voltammetry is shown in tab. 1. The line resistance at hot state between two phases derived from the voltammetry is 0.1964 Ω.

Table 1. Line resistance at cold state between two phases

	U-V[Ω]	V-W[Ω]	W-U[Ω]
First	0.1507	0.1507	0.1508
Second	0.1507	0.1507	0.1508
Third	0.1508	0.1507	0.1508
Mean resistance	0.1507	0.1507	0.1508
Equivalent resistance at 20 ºC	0.1447	0.1447	0.1448

The temperature of the coils at cold state is 44.1 ºC, and the ambient temperature at inlet is 38.5 ºC after running. Then the temperature rise of stator coils is 90 K according to the eq. (1):

$$\Delta\theta = \frac{R_N - R_C}{R_C}\left(K_1 + \theta_c\right) + \theta_c - \theta_h \tag{1}$$

where K_1 is a constant, 234.5, R_N – the line resistance at hot state, R_C – the line resistance at cold state, θ_c – the temperature of stator coils at cold state, and θ_h – the ambient temperature at inlet of the motor after the power is cut off.

Embedding thermal resistors

The location of the measuring points, namely the location where the thermal resistors are buried are shown in fig. 2.

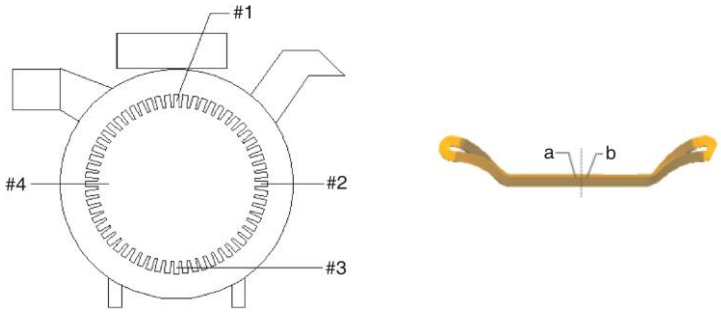

Figure 2. (a) Location of the resistors in longitudinal section (b) location of the resistors in cross-section

The related parameters are measured and shown in tab. 2. The local temperature is measured by embedding thermal resistors, which is shown in tab. 3.

Table 2. Related parameters measured

Parameter	Value
Voltage between lines, [V]	1102.6
Current, [A]	127.6
Frequency, [Hz]	68.0
Input power, [kW]	210.5
Output power, [kW]	200.5
Torque, [Nm]	948
Speed [rmin^{-1}]	2020
Temperature of air at entrance [℃]	44.1
Temperature of air at exit [℃]	62.2
Ambient temperature [℃]	37.9

Table 3. Local temperature of stator coils

Location	Point a, [℃]	Point b, [℃]	Average temperature, [℃]
#1	139.3	139.7	139.5
#2	136.0	136.3	136.2
#3	145.8	145.2	145.5
#4	144.7	145.6	145.2

Numerical simulation

The temperature rise of motor is also investigated in numerical method to observe the temperature field of the whole motor, containing the rotor and stator.

Model description and computational methods

In order to simplify the practical model, some necessary simplification is done to get the solution domain. Firstly, peripheral parts are deleted, such as screws, bolts, shims, holes, electrical junction box, support components, end-plates, platens, and oil seals. Secondly, plenty of edge rounding and fillets are deleted. Thirdly, the features on assemblies and sub-assemblies are moved to corresponding parts. Fourthly, the 3-D tortuous stator coils which are close to each other at the end links are simplified rationally. All parts are simplified under the principle of having little influence on flow field. Fifthly, the insulating covered the stator coils are deleted and the wall between the stator coils and stator core whose thermal resistance is equivalent to insulating material is set up in FLUENT. Sixth, the small size deviations between two adjacent parts are eliminated. Seventh, the assembling gaps, and the interference on parts and between two adjacent parts are removed. Then, the simplified motor model is obtained.

As the rotor, the fan and other parts are rotational, the multiple frame motion model is adopted. According to the multiple frame motion model, the fluid zone is divided into rotational part and stationary part.

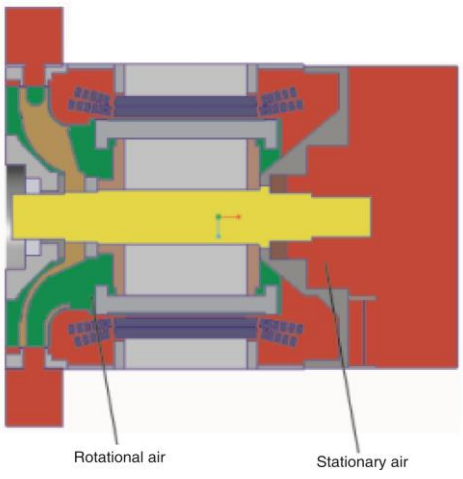

Figure. 3 Solution domain

The motor model and the fluid zone compose the solution domain, shown in fig. 3. As the model is not symmetrical totally, not the quarter but the whole model is taken as the solution domain.

The discretization of solution domain is achieved by means of unstructured mesh. In order to make the mesh nodes between two adjacent bodies coincide at the interface, all the bodies compose a new part. The body mesh size of solid zone is 8 mm and the size of liquid zone is 5 mm. The inflation is created at the air passage inside the rotor core. The generated mesh is made up of 30 million finite volumes. The grid created are shown in fig. 4. The mesh quality is larger than 0.38 and the skewness is less than 0.75, which meets the engineering requirements to mesh.

This paper focuses on temperature field at not starting-up or shutting down process but running state. So it is taken for a steady problem.

The intensity of the flow and heat transfer at the gap between the stator and the rotor influences directly the cooling, safe operation and the lifespan of the motor. [15] The rated speed is 2014 r/min and the Reynolds number could be derived by eq. (2):

$$\mathrm{Re} = \frac{ud}{\nu} = \frac{20 \cdot 0.33}{18.80 \cdot 10^{-6}} = 351064 \qquad (2)$$

where u is the velocity of the air in the gap, d – the diameter of the gap, and ν – the dynamic viscosity of the air.

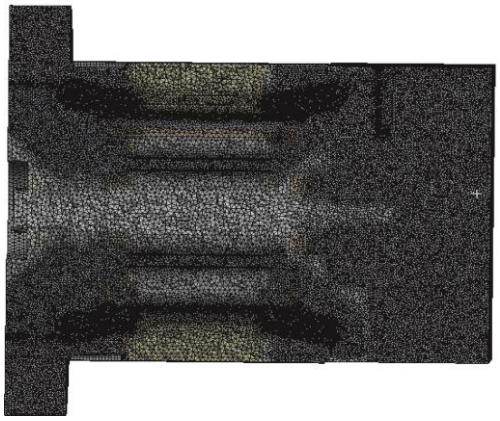

Figure. 4 Schematic diagram of grid division

The highest speed of the motor is 4025 r/min and the Reynolds number is nearly double. Therefore, the flow in motors is a typical engineering turbulent flow. The standard k-ε model has been the workhorse of practical engineering flow calculations in the time. Because of its robustness, economy, and reasonable accuracy, it is popular for a wide range of turbulent flows, especially industrial flow and heat transfer simulations [16]. The computational complexity will be huge if the k-ω model or the SST model be adopted and the corresponding mesh will be unrealizable. Most studies on thermal analysis of motors chose standard k-ε model [15, 17-20]. So the standard k-ε model is adopted.

The zone near wall is treated by standard wall functions. The multiple frame motion is adopted to tackle the rotational part such as the rotor, shaft, and fan. The loss of the motor is the difference between the input power and the output power. The loss is the source term in the energy equation.

As the core is piled up by pieces of silicon steel sheet which is covered with insulting paint. So the thermal conductivity of the core is cylindrical orthotropic. In detail, the thermal conductivity in axial direction is 0.2 W/mK and the thermal conductivity in radial and circumferential direction is 40 W/mK. The air around the running motor is 37.9 ºC and its density, thermal conductivity, and viscosity are all linearly with temperature in the range of the air temperature 20-60 ºC in the simulation process. The variation of specific heat of air and thermal properties of other insulating and metal material can be neglected.

As the motor is self-ventilation, the mass-flow and velocity at inlet are determined by the rotational speed. So the boundary conditions at inlet and outlet are set as pressure-inlet and pressure-out, respectively. The outside surfaces of the crate are set as convective boundary condition. The type of the face between the rotational air zone and the stationary air zone is taken for interior. Others are set wall boundary condition where the momentum condition is no slip and the thermal condition is wall-coupled. All the boundary conditions are shown in fig. 5.

The pressure-velocity coupling method is the SIMPLE algorithm. The diffusion terms are the second-order central-difference and the convective terms are second-order upwind to reduce the numerical diffusion.

Grid independence test and model validation

Before proceeding further, the grid used for present study is checked at first. Unstructured tetrahedral grids are used. Totally, four sets of grid are taken to do grid independent

test. The variations of the mass-flow rate of air and the total heat flux with the grid number are presented in fig. 6 where ϕ is the heat flux and q_m is the mass-flow rate.

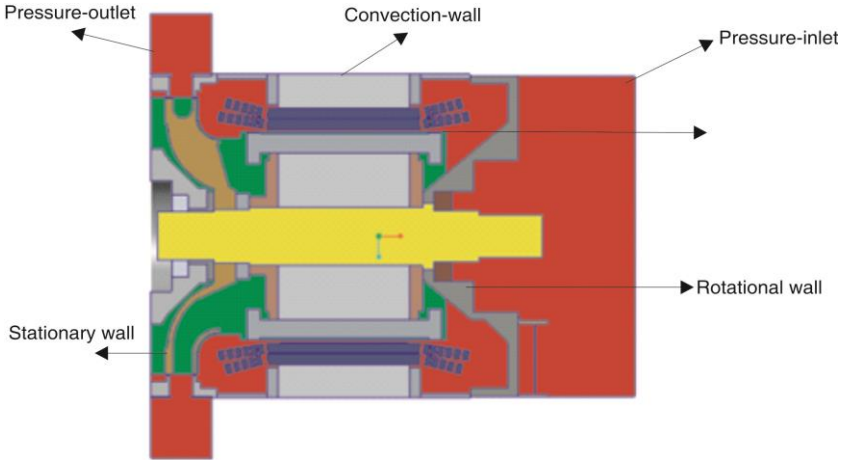

Figure 5. Schematic diagram of boundary condition

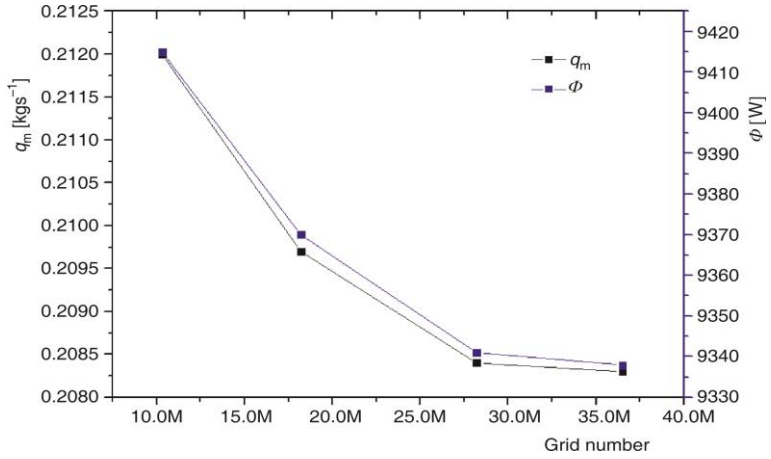

Figure 6. Grid independent test

As the variation of the mass-flow rate of air and total heat flux when the grid increases from 28.0 million to 37.2 million is less than 2%, the grid with 28 million finite volumes is adopted in the following calculation.

In order to validate the model, the measured temperature in the experiment and the calculated temperature numerically are contrasted in tab. 4.

Table 4. Numerical result and relative error

Location	Experimental results, [ºC]	Numerical results, [ºC]	Relative error, [%]
#1	139.5	133	4.7
#2	136.2	128	6.0
#3	145.5	134	7.9
#4	145.2	141	2.9

Comparing the two results, the temperature measured in experiment is a little higher than the temperature simulated. It is found that the maximal error is 7.9%, which proves that the numerical model is reasonable and robust.

Results and discussion

The velocity and temperature contour of the longitude section are shown in figs. 7(a) and 7(b), respectively.

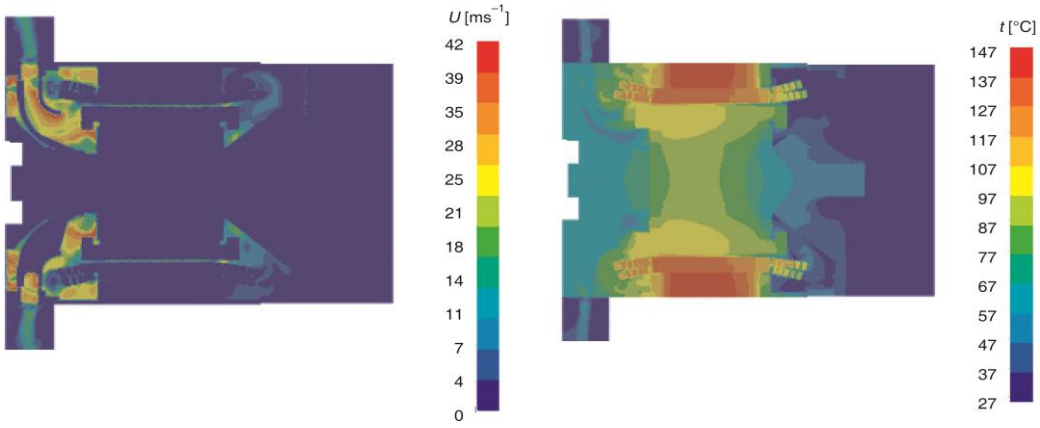

Figure 7. (a) Velocity, *U*, contour of the longitude section, (b) temperature, *t*, contour of the longitude section

As we can see from fig. 7(a), the velocity around the fan, especially the tip, is the biggest, about 40 m/s. The air around the end of the coils has a specific speed, about 10 m/s, which can be cooled well. Figure 7(b) shows that the temperature of the stator is higher than the rotor. Because the axial heat conduction at the rotor is strong and there are 12 holes for wind to enhance the convective heat transfer of rotor. As for the stator, it is hard for the heat release from the exterior of the stator [21]. The temperature of the point at the non-driving end with a distance of 25 mm to the middle cross-section is the highest, 143 ºC, because the temperature of the air at the non-driving end is higher than the driving end. The highest temperature is lower than the allowed highest temperature of the insulating degree, H, so there is no over-temperature danger when the motor runs at rated condition.

Factors sensitivity analysis

Because not the optimization but the sensitivity analysis is concerned in the research on the thermal analysis of the motor, the Taguchi's method other than the particle swarm optimization or genetic algorithms is adopted.

Taguchi method is a low cost and high benefit method to find out the sensitive parameter. The orthogonal test technique advocated by Taguchi method can significantly reduce the number of tests. The essence of Taguchi's method is to solve the signal-to-noise ratio (SNR) of the index function through a set of orthogonal combinations including multiple influencing factors and horizontal numbers, so as to judge the advantages and disadvantages and weights of each influencing factor [22, 23]. It is widely used in the scientific experimental researches.

Here, the eight critical parameters in models are mainly investigated. Seven of them are set three levels and one is set two levels in their common range. Normally, $7^3 \times 1^2 = 686$

models need to be calculated. But by means of Taguchi method, only eighteen models should be calculated [24]

In the whole, this work applies the Taguchi method with the orthogonal array table of $L_{18}(7^3\times1^2)$. There are 18 tests in the orthogonal array. Every test is solved by the CFD simulation. Namely, the Taguchi method is coupled with the CFD.

Tests arrangement

The design parameters values are shown as tab. 5.

The copper loss in tab. 5 is the power consumed by the resistance of the windings when current passes through the windings of the stator and rotor. When motors operate, eddy currents are generated inside the iron core, and when the eddy current passes through the iron core, heat is generated inside the iron core, which consumes energy and is named iron loss.

Table 5. Design parameters values

Symbol	Factor [unit]	Level 1	Level 2	Level 3
R_C	Contact thermal resistance, [m^2KW^{-1}]	0	0.0004	–
S_{Cu}	Copper loss, [Wm^{-3}]	400000	440000	480000
S_{Fe}	Iron loss, [Wm^{-3}]	120000	160000	200000
δ	Thickness of the insulating layers, [mm]	1	2	3
h	Outside convection heat transfer coefficient of crate, [$Wm^{-2}K^{-1}$]	5	12.5	20
λ_{ins}	Thermal conductivity of the insulation, [$Wm^{-1}K^{-1}$]	0.13	0.165	0.2
λ_l	Thermal conductivity of the core in axial direction, [$Wm^{-1}K^{-1}$]	1	1.5	2
t_f	Ambient temperature, [ºC]	25	35	45

As shown in tab. 5, the contact thermal resistance 0.0004 Wm^2/K is the value between two pieces of stainless steel material [25]. The different values of the copper loss and the iron loss at the tooth in tab. 5 obtained by various methods are all at the rated condition, namely, at 2014 r/min. The thickness of the insulating layers and the outside convection heat transfer coefficient of crate are set as the possible values. The Level 3 of thermal conductivity of the insulation is the common value and the Level 1 is the value when the insulation ages [25]. Because the thermal conductivity of the insulation decreases with utility time going on. Thermal conductivity of the core in axial direction are set as different values because the manufacturing technology and the pressure are different. The ambient temperature are the common values all around the year.

In the present study, eighteen numerical simulation tests are conducted as depicted in tab. 6.

The insulation around the stator windings is the weakest part during the motor running process. Because if the actual temperature of the insulation is higher than its maximal temperature allowed, the insulation will breakdown. Approximately, this study takes the tem-

Table 6. Orthogonal array table of $L_{18}(7^3\times1^2)$ and effect of all cases

R_c	S_{Cu}	S_{Fe}	δ	h	λ_{ins}	λ_l	t_f	t_{max}	SNR_{tmax}	$\Delta\theta$	$SNR_{\Delta t}$
[m^2KW^{-1}]	[Wm^{-3}]	[Wm^{-3}]	[mm]	[$Wm^{-2}K^{-1}$]	[$Wm^{-1}K^{-1}$]	[$Wm^{-1}K^{-1}$]	[ºC]	[ºC]	[–]	[K]	[–]
0	400000	120000	1	5.0	0.13	1.0	25	110.6	–40.9	85.6	–38.6
0	400000	160000	2	12.5	0.17	1.5	35	122.3	–41.7	87.3	–38.8
0	400000	200000	3	20.0	0.20	2.0	45	133.3	–42.5	88.3	–38.9
0	440000	120000	1	12.5	0.17	2.0	45	128.9	–42.2	83.9	–38.5
0	440000	160000	2	20.0	0.20	1.0	25	112.3	–41.0	87.3	–38.8
0	440000	200000	3	5.0	0.13	1.5	35	143.9	–43.2	108.9	–40.7
0	480000	120000	2	5.0	0.20	1.5	45	142.0	–43.0	97.0	–39.7
0	480000	160000	3	12.5	0.13	2.0	25	132.6	–42.5	107.6	–40.6
0.0004	480000	200000	1	20.0	0.17	1.0	35	126.1	–42.0	91.1	–39.2
0.0004	400000	120000	3	20.0	0.17	1.5	25	110.9	–40.9	85.9	–38.7
0.0004	400000	160000	1	5.0	0.20	2.0	35	119.6	–41.6	84.6	–38.5
0.0004	400000	200000	2	12.5	0.13	1.0	45	138.4	–42.8	93.4	–39.4
0.0004	440000	120000	2	20.0	0.13	2.0	35	123.9	–41.9	88.9	–39.0
0.0004	440000	160000	3	5.0	0.17	1.0	45	145.7	–43.3	100.7	–40.1
0.0004	440000	200000	1	12.5	0.20	1.5	25	115.0	–41.2	90.0	–39.1
0.0004	480000	120000	3	12.5	0.20	1.0	35	133.1	–42.5	98.1	–39.8
0.0004	480000	160000	1	20.0	0.13	1.5	45	133.2	–42.5	88.2	–38.9
0.0004	480000	200000	2	5.0	0.17	2.0	25	130.8	–42.3	105.8	–40.5

perature of the stator windings as a substitute of the temperature of the insulation. Because the insulation is too thin to be established. The SNR ratio is usually used in engineering and experimental design [26, 27]. The SNR is defined by the following equations [28]:

$$SNR_{t_{max}} = -\log\left(\frac{1}{t_{max}^{\ 2}}\right) \tag{3}$$

$$SNR_{\Delta t} = -\log\left(\frac{1}{\Delta t^2}\right) \tag{4}$$

Contribution ratio

Here, the corresponding SNR of the highest temperature and temperature rise of stator coils all the tests are shown in tab. 7. The rank R and the distributed ratio CR can be defined by:

$$R_j(j = 1,2,\cdots;8) = \frac{\max\{SNRi|i = 1,2,3\}}{2} - \frac{\min\{SNRi|i = 1,2,3\}}{2} \tag{5}$$

$$CR_j = \frac{R_j}{\sum_{j=1}^{7} R_j} \tag{6}$$

Table 7. Factorial effect and contribution ratio

	t_{max}					$\Delta\theta$				
	SNR_1	SNR_2	SNR_3	R	CR	SNR_1	SNR_2	SNR_3	R	CR
R_c	–379.0	–378.9	–	0.08	0.32%	–354.0	–354.0	–	0.00	0.01%
S_{Cu}	–250.4	–252.7	–254.8	4.42	17.76%	–233.0	–236.2	–238.8	5.77	24.76%
S_{Fe}	–251.4	–252.5	–254.0	2.67	10.73%	–234.4	–235.8	–237.8	3.48	14.93%
δ	–250.4	–252.8	–254.8	4.41	17.71%	–232.9	–236.3	–238.9	6.01	25.79%
h	–254.2	–252.9	–250.8	3.47	13.94%	–238.2	–236.3	–233.5	4.73	20.27%
λ_{ins}	–253.7	–252.5	–251.8	1.86	7.47%	–237.3	–235.7	–234.9	2.38	10.21%
λ_l	–252.5	–252.6	–252.9	0.43	1.72%	–236.0	–236.0	–236.0	0.08	0.36%
t_f	–248.8	–252.8	–256.3	7.55	30.34%	–236.4	–236.1	–235.5	0.85	3.66%

According to the contribution ratios in fig. 8, the contribution ratios to the highest temperature are similar to the highest temperature rise of stator coils, except for the effect of the ambient temperature, which has the biggest effect to the highest temperature and little effect to the temperature rise. It is reasonable because the temperature rise is the difference of the windings temperature and the ambient temperature at the entrance. The copper loss and the thickness of the insulating layers have the dominant effect to both the temperature and the temperature rise. Then the outside convection heat transfer coefficient of crate, the iron loss at the tooth and thermal conductivity of the insulation are in order. The contact thermal resistance and the thermal conductivity of the core in axial direction have little contribution, which can be neglected.

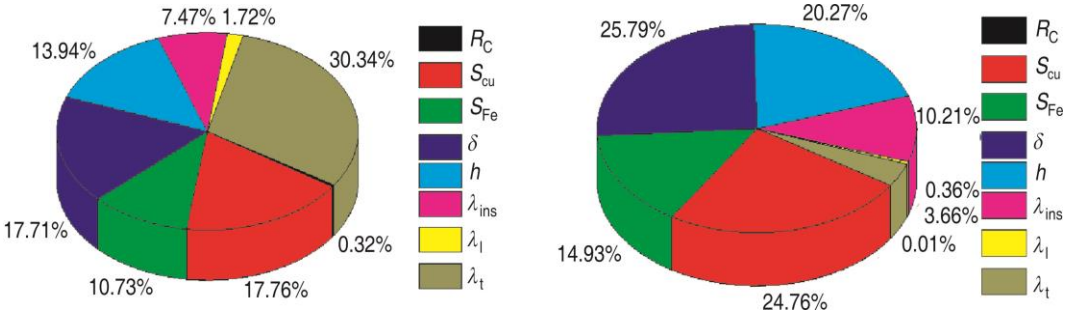

Figure 8. (a) Contribution ratio to maximal temperature (b) contribution ratio to maximal temperature rise (*for colour image see journal web site*)

Conclusions

In this article, both the experimental research and numerical calculation are carried out to investigate the temperature of the motor. Eighteen tests are conducted by combined CFD-Taguchi method in order to perform the sensitivity analysis to the highest temperature of the metro motor. Major findings are summarized as follows.

- Firstly, the maximal temperature and the maximal temperature rise at rated speed are 143 ºC and 99 K, respectively, according to the numerical results. The values are 145.8 ºC and 90 K, according to the experimental result, which are lower than the temperature allowed, 180 ºC and temperature rise limit, 125 K.

- Secondly, the key factors influencing the temperature are in sequence the ambient temperature, the copper loss, the thickness of the layers, the outside convection heat transfer coefficient of crate, the iron loss at the tooth and thermal conductivity of the insulation. The contact thermal resistance and the thermal conductivity of the core in axial direction has little influence to the temperature. The rank to the temperature rise is similar except the ambient temperature, which has little effect to the temperature rise.

Acknowledgment

This study is supported by the project of Yongji Zhongche Motor Co. Ltd (201901107) and the Foundation for Innovative Research Groups of the National Natural Science Foundation of China (No.51721004).

Nomenclature

h – heat transfer coefficient, [$Wm^{-2}K^{-1}$]
q_m – mass-flow rate
R_N – line resistance at hot state, [Ω]
R_C – line resistance at cold state, [Ω]
Rc – contact thermal resistance,[m^2KW^{-1}]
S_{Cu} – copper loss, [Wm^{-3}]
S_{Fe} – iron loss at the tooth, [Wm^{-3}]
t_f – ambient temperature, [℃]
t_{max} – maximal temperature of stator coil, [℃]

Greek symbols

δ – thickness of the insulating layers, [mm]
θ_c – temperature of stator coils at cold state, [℃]
θ_h – ambient temperature at inlet after the power is cut off, [℃]
$\Delta\theta$ – average temperature of stator coil, [K]
λ_{ins} – thermal conductivity of insulating material, [$Wm^{-1}K^{-1}$]
λ_l – thermal conductivity of the core in axial direction , [$Wm^{-1}K^{-1}$]
Φ – total heat flux, [W]

Subscripts

i – the level
j – the factor
ins – insulating material
L – axial direction
C – state before running
N – state after running
h – state after the power is cut off

References

[1] Wenbo, W., Lumped-Parameter Thermal Model Analysis for PMSM (in Chinese), Ph. D. thesis, Zhejiang University, Hangzhou, China, 2015
[2] Živan, T. S., *et al.* , Temperature Rise in Induction Motor Windings as the Cause of Variation in Rotational Speed of an Axial Fan, *Temperature Science, 20*, (2016), Suppl. 5, pp. S1449-S1459
[3] Meng, D. W., *et al.* , Calculation of Temperature Rise for High-Voltage Induction Motor with Compact Type in Starting Process, *Applied Mechanics and Materials*, *705* (2015), 10, pp , 232-236
[4] Wen, J. B., *et al*., Synthetic Calculation for the Ventilation and Heating of Large Water Wheel Generator (in Chinese), *Proceedings of the CSEE*, *20* (2000), 11, pp. 6-9
[5] Claudio, S., *et al*., Analytical Thermal Model for Fast Stator Winding Temperature Prediction, *Transactions on Industrial Electronics*, *64* (2017), 8, pp. 6116-6126
[6] Zhang, C., *et al*., A Discrete Algorithm for Overload Protection Principle, *Applied Mechanics and Materials*, *543-547* (2017), 8, pp. 1219-1222
[7] Zhang, C., *et al*., Research on Real-time Losses for Sensor less Motor Temperature Identification Based on Thermal Network Model, *Proceedings*, 1th International Conference on Electronics Instrumentation and Information Systems, Harbin, China, 2017
[8] Bogumi, M., *et al*., Thermal Calculations and Tests of Brushless Motor with Liquid-cooled Frame, *Przeglad Elektrotehniczny*, *93* (2017), 2, pp.19-22
[9] Yabiku, R., *et al*., Use of Thermal Network on Determining the Temperature Distribution Inside Electric Motors in Steady State and Dynamic Conditions, *Proceedings*, Petroleum and Chemical Industry Conference, Anaheim, Cal., USA, 2009, Vol. 46, pp. 1787-1795
[10] Hirano, S., *et al*., Estimation of Heat Transfer Property among Parts on EV Motor using Thermal Network Method, *Transaction of the Japan of Mechanical Engineering, 81* (2015), 822, pp. 307-317

[11] Mohamed, A. F., *et al*., Thermal Analysis of a Permanent Magnet Synchronous Motor for Electric Vehicles, *Journal of Asian Electric Vehicles*, *6* (2014), 2, pp. 1145-1151
[12] Zhu, S., *et al*., Direct Coupling Method for Coupled Field-Circuit Thermal Model of Electrical Machines, *Transactions on Energy Conversion*, *33* (2018), 6. pp. 473-482
[13] Kim, S., *et al*., Optimization for Reduction of Torque Ripple in Interior Permanent Magnet Motor by Using the Taguchi Method, *Transactions on Magnetics*, *41* (2005), 5, pp. 1796-1799
[14] Wang, H. T., *et al*., Application of Taguchi Method to Robust Design of BLDC Motor Performance, *Transaction on Magnetics*, *35* (1999), 5, pp. 3700-3703
[15] Jiade, H., *et al*.,. Research on Taylor Vortex's Flow and Heat Transfer Characteristics of the Air Gap of the Motor (in Chinese), *Journal of Harbin University of Science and Technology. 23* (2018), 2, pp. 114-119
[16] Launder, B. E., *et al*. *Lectures in Mathematical Models of Turbulence*. Academic Press, London, UK. 1972
[17] Sung-Hyun, M., *et al*.,.Thermal-Flow Analysis and Cooling Performance Enhancement of a Totally Enclosed Fan-Cooled Motor, *Proceedings*, International Conference on Electrical Machines and Systems, Busan, Korea, 2013, Vol. 10, pp. 26-29
[18] Yiping, L., *et al*.,. Simulation and Analysis of Thermal Fields of Rotor Multislots for Nonsalient-Pole Motor, *Transaction on Industrial Electronics*. 62 (2015),12, pp. 7678-7686
[19] Tian, H., *et al*.,. Calculation of 3D Fluid Flow Field and Thermal Field of Air-Cooled Medium Motor, *Applied Mechanics and Materials*, *513-517* (2014), 6, pp. 3468-3471
[20] Jinling, Z., *et al*., Thermal Simulation of an Oil-Cooled Permanent Magnet Synchronous Motor, *Proceedings*, International Electric Machines and Drives Conference, Miami, Fla., USA, 2017, Vol. 4
[21] Xueqi, L., *et al*., Numerical Simulation and Experimental Investigation of Heat Transfer Characteristics for a Metro Motor (in Chinese), *Journal of Xi'an Jiaotong University*, 52 (2018), 6, pp. 148-154
[22] Roy, R., *A Primer on the Taguchi Method*, 2nd edition, Society of Manufacturing Engineers Press, New York, USA, 2010
[23] Hossein, M. K., *et al*., Electrospinning of Polymethyl Methacrylate Nanofibers: Optimization of Processing Parameters Using the Taguchi Design of Experiments, *Textile Research Journal*, *85* (2014), 4, pp. 1-13
[24] Zhijun, H., *Three Stage Design* (in Chinese), China Machine Press, Chengdu, China, 1992
[25] Deji, L., *Thermal Analysis Calculation and Application of Motor* (in Chinese), Sichuan University Press, Chengdu, China, 1994
[26] Taguchi, G., *et al*., *Quality Engineering in Production Systems*, McGraw-Hill, New York, USA, 1989
[27] Xueqi, L., *et al*., Thermal Field Numerical Calculation of Motor and Correlated Factors Sensitivity Analysis using combined CFD-Taguchi method, *Proceedings*, 11th International Conference on Computational Heat, Mass and Momentum Transfer, Cracow, Poland, 2018, Vol. 5
[28] Tsai, J. T., *et al*., Hybrid Taguchi-Genetic Algorithm for Global Numerical Optimization, *Transactions on Evolutionary Computation*, *8* (2004), 4, pp. 365-377

Paper submitted: August 14, 2018
Paper revised: October 15, 2018
Paper accepted: January, 2019